# Solar photothermochemical alkane reverse combustion

Wilaiwan Chanmanee[a], Mohammad Fakrul Islam[a], Brian H. Dennis[b,1], and Frederick M. MacDonnell[a,1]

[a]Department of Chemistry and Biochemistry, University of Texas at Arlington, Arlington TX 76019; and [b]Department of Mechanical and Aerospace Engineering, University of Texas at Arlington, Arlington TX 76019

Edited by Alexis T. Bell, University of California, Berkeley, CA, and approved January 21, 2016 (received for review August 25, 2015)

**A one-step, gas-phase photothermocatalytic process for the synthesis of hydrocarbons, including liquid alkanes, aromatics, and oxygenates, with carbon numbers ($C_n$) up to $C_{13}$, from $CO_2$ and water is demonstrated in a flow photoreactor operating at elevated temperatures (180–200 °C) and pressures (1–6 bar) using a 5% cobalt on $TiO_2$ catalyst and under UV irradiation. A parametric study of temperature, pressure, and partial pressure ratio revealed that temperatures in excess of 160 °C are needed to obtain the higher $C_n$ products in quantity and that the product distribution shifts toward higher $C_n$ products with increasing pressure. In the best run so far, over 13% by mass of the products were $C_5$+ hydrocarbons and some of these, i.e., octane, are drop-in replacements for existing liquid hydrocarbons fuels. Dioxygen was detected in yields ranging between 64% and 150%. In principle, this tandem photochemical–thermochemical process, fitted with a photocatalyst better matched to the solar spectrum, could provide a cheap and direct method to produce liquid hydrocarbons from $CO_2$ and water via a solar process which uses concentrated sunlight for both photochemical excitation to generate high-energy intermediates and heat to drive important thermochemical carbon-chain-forming reactions.**

solar fuel | $CO_2$ reduction | water splitting | photochemistry | Fischer–Tropsch

Oil is essential for sustaining the current global population and economy because it is the primary source of transportation fuels. Diesel, jet, and gasoline hydrocarbon fuels are unrivaled in terms of energy density and ease of use and storage; however, as fossil fuels their combustion leads to a significant anthropogenic contribution of $CO_2$ to the atmosphere, estimated at $40 \times 10^9$ metric tons of $CO_2$ in 2012 alone (1, 2). The eventual replacement of oil with fuels generated from sustainable and carbon-neutral sources is necessary if we are to avoid harmful climate change due to the buildup of greenhouse gases in the atmosphere (3). Advances in solar-based technologies are the most promising (4); however, these technologies generally produce either electricity or hydrogen, neither of which is an ideal replacement for liquid hydrocarbons. The least disruptive technology would replace oil-derived hydrocarbons with liquid hydrocarbon fuels derived from $CO_2$, water, and a clean energy source, such as the sun, leading to a carbon-neutral fuel cycle (5–7).

Currently, there are a number of promising strategies to harness solar energy to generate high-energy molecules (fuels) from water and/or carbon dioxide, including (*i*) high-temperature thermochemical cycles (8), (*ii*) coupling photovoltaics to water electrolysis (PV-EC) (9, 10), (*iii*) developing single or tandem photoelectrochemical cells (PEC) (11–13), or (*iv*) direct photochemical methods (PC) using semiconductor materials, often modified by added cocatalysts or nanostructuring techniques (12, 14, 15). Hydrogen, carbon monoxide, $C_1$ hydrocarbons, and syngas are the most commonly produced fuels and are derived from water or water and $CO_2$ (6, 16, 17). Hydrogen produced via the water-splitting reaction (WSR, reaction **1**) is arguably the easiest to produce and stores the most energy on a mass basis (kJ/kg); however, it is not a particularly attractive replacement fuel for transportation, due to technological issues with low-volume energy density, safe storage, and transportation (18). Moreover, switching to a hydrogen-based transportation fuel would also require a considerable investment in upgrading the existing automotive fleet and fuel distribution infrastructure.

One commonly proposed solution to this dilemma is to use the $H_2$ generated via the WSR, reaction **1**, in combination with $CO_2$ to synthesize liquid hydrocarbon fuels, using the reverse water–gas shift (RWGS), reaction **2**, and Fischer–Tropsch synthesis (FTS), reaction **3**. The combination of reactions **1**–**3** is the reverse of

$$H_2O \rightarrow H_2 + 1/2O_2 \quad \Delta G^\circ = 237.3 \text{kJ/mol} \quad (\textbf{WSR}), \qquad [1]$$

$$CO_2 + H_2 \rightleftharpoons CO + H_2O \quad \Delta G^\circ = 25.2 \text{kJ/mol} \quad (\textbf{RWGS}), \qquad [2]$$

$$(2n+1)H_2 + n\ CO \rightarrow C_nH_{(2n+2)} + n\ H_2O \quad \Delta G^\circ \sim -99\ \text{n kJ/mol} \quad (\textbf{FTS}), \qquad [3]$$

$$(\text{n}+1)H_2O + \text{n}\ CO_2 \rightarrow C_nH_{2n+2} + (3/2\text{n} + 1/2)O_2 \quad \Delta G^\circ \sim 665\ \text{n kJ/mol} \quad (\textbf{ARC}) \qquad [4]$$

combustion and, as generally proposed, would be carried out as separate unit operations, each with its attendant efficiency losses and capital and operating costs (19, 20). We report here a photothermochemical process for driving the alkane reverse combustion (ARC) reaction (reaction **4**) to produce $C_1$ to $C_{13}$ hydrocarbons in a single operation unit. If the process was driven by the sun to provide both photons and heat, a solar photothermochemical alkane reverse combustion (SPARC) process could be achieved in one step. If the SPARC reaction could be optimized to predominantly produce liquid hydrocarbons, and these products were derived from atmospheric $CO_2$, a sustainable and carbon-neutral liquid fuel cycle could be realized.

The direct production of $C_1$ hydrocarbons such as methane, methanol, formic acid, and CO from $CO_2$ and water in a photoelectrochemical reactor was realized as early as the mid 1970s when Halmann (21) and then Inoue et al. (22) showed that irradiation of $TiO_2$-coated electrode suspended in $CO_2$-saturated aqueous

## Significance

**An efficient solar process for the one-step conversion of $CO_2$ and $H_2O$ to $C_5$+ liquid hydrocarbons and $O_2$ would revolutionize how solar fuel replacements for gasoline, jet, and diesel solar fuels could be produced and could lead to a carbon-neutral fuel cycle. We demonstrate that this reaction is possible in a single-step process by operating the photocatalytic reaction at elevated temperatures and pressures. The process uses cheap and earth-abundant catalytic materials, and the unusual operating conditions expand the range of materials that can be developed as photocatalysts. Whereas the efficiency of the current system is not commercially viable, it is far from optimized and it opens a promising new path by which such solar processes may be realized.**

Author contributions: W.C., B.H.D., and F.M.M. designed research; W.C. and M.F.I. performed research; W.C., M.F.I., B.H.D., and F.M.M. analyzed data; and W.C., B.H.D., and F.M.M. wrote the paper.

The authors declare no conflict of interest.

This article is a PNAS Direct Submission.

[1]To whom correspondence may be addressed. Email: dennisb@uta.edu or macdonn@uta.edu.

This article contains supporting information online at www.pnas.org/lookup/suppl/doi:10.1073/pnas.1516945113/-/DCSupplemental.

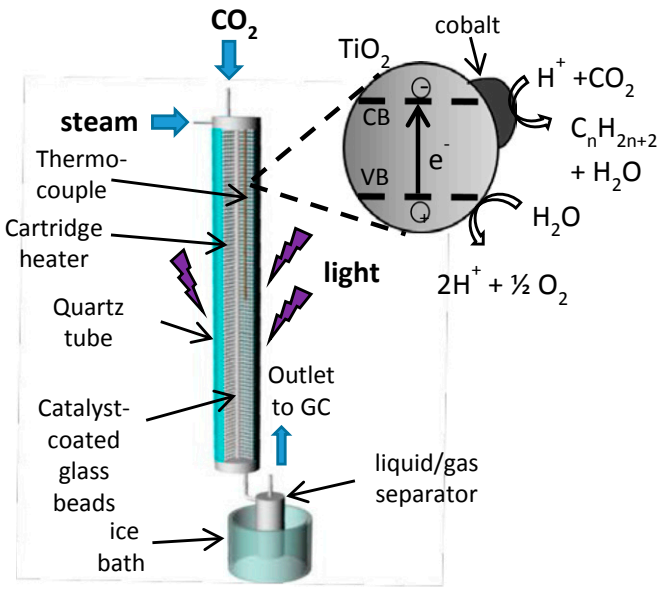


**Fig. 1.** Schematic diagram of photothermal flow reactor with cartoon picture of a single Co/$TiO_2$ particle undergoing catalysis and TEM picture of cobalt on P25 $TiO_2$ catalyst.

solutions yielded a number of $C_1$ products. Since this time, research has largely focused on the exploration and development of new semiconductor photocatalysts (23), modifications of the semiconductor catalyst in the form of added cocatalysts, e.g., Ni, Cu, Ag, and Pt (23–25), new methods to nanostructure the catalyst (26), and the coupling of molecular dyes and cocatalysts with the heterogeneous catalyst (27, 28). Whereas these advances have led to improvements in catalytic efficiency and quantum yields, little progress has been realized in extending the selectivity of the reaction to favor the more desirable, higher carbon number liquid hydrocarbons (29). Although reports of trace amounts of products, such as ethane, ethanol, acetic acid, propanol, and butanol, are not unknown (30–34), they are the exception and frequently the underlying cause for their generation is unknown. Of these reports, the work of Roy et al. (35) and Varghese et al. (36) stands out. They reported that high-temperature-annealed $TiO_2$ nanotubes modified with Pt, Pd, or Cu not only gave methane, but also traces of ethane, propane, butane, pentane, and hexane as well as olefins and branched paraffins, although the details regarding product quantification and characterization were omitted. Whereas this work yielded the highest $C_n$ products yet reported, the results contributed little toward a mechanistic understanding as to how to deliberately target these products.

Thus, despite over 40 y of research on the photochemical $CO_2$ reduction with semiconductors, no clear method for directly producing $C_5$+ liquid hydrocarbon products exists. Herein, we demonstrate that operation of the photochemical ARC reaction at elevated temperatures in the presence of a hybrid FTS-like photocatalyst (cobalt on $TiO_2$ support) directly yields $C_2$+ hydrocarbons as the dominant products, including a significant portion of $C_5$+ liquid hydrocarbons. The key insights are that: (*i*) even though the FTS reaction is exothermic, a minimum temperature of ~180 °C is required to obtain reasonable kinetics for the carbon-chain-forming process (37, 38) and (*ii*) the majority of metals (i.e., Ni, Pd, Pt, Cu) used for $CO_2$ photocatalytic hydrogenation are poor FTS catalysts as they favor $C_1$ products (39). Fe, Co, and Ru are commonly used as FTS catalysts because they exhibit high $C_n$ selectivity (39), but they have not been commonly explored in the context of $CO_2$ photoreduction/hydrogenation. By operating the SPARC reaction at elevated temperature and pressure over a hybrid FTS photocatalyst, the products of the photocatalytic reaction can be consumed in thermal reactions which favor higher $C_n$ products.

## Results and Discussion

To examine the SPARC reaction as a function of temperature and pressure, we constructed a fixed-bed, tubular flow reactor in which the catalyst bed could be both heated and irradiated, as shown schematically in Fig. 1. During the reaction, $CO_2$ and steam were flowed at 40 standard cubic centimeters per minute (sccm) over the 5% cobalt on a $TiO_2$ catalyst bed, which was heated via an internal electric heater and irradiated with four surrounding 250-W Hg lamps. The products were collected by passing the hot effluent gas through a condenser unit at 0 °C to capture condensable products, through a back-pressure regulator to drop the pressure to 1.0 bar, and then through a sampling loop of an automated online gas chromatograph for real-time gas analysis (full details in the *SI Appendix*).

As shown in Fig. 2, the condensable (liquid) productivity increases upon increasing the temperature from 110 to 200 °C (1 bar, $P_{H2O}/P_{CO2}$ = 1.2, UV irradiation) and the product distribution shifts to $C_2$ ($CH_3CH_2OH$ and $CH_3COOH$) and $C_3$ (propanol) products. Temperatures higher than 200 °C were not explored due to reactor limitations. Below 150 °C, methanol is the exclusive condensable product, whereas at 150 °C or above, $C_2$ and $C_3$ products become more prevalent and the methanol diminishes. Upon going from 180 to 200 °C, there was doubling of the mass productivity but a drop in propanol production and a large increase in acetic acid formation. Upon lowering the $P_{H2O}/P_{CO2}$ to 0.6 (1 bar, 200 °C, UV irradiation) the amount of propanol increased 14-fold and pentanol ($C_5H_{12}O$) was also detected. The appearance of the heavier alcohols at or above 150 °C is consistent with an FTS-like mechanism becoming active as the thermal energy approaches the activation energy needed for chain formation (37, 38, 40). In a related study of the effect of temperature on the photochemical reduction of $CO_2$ to methane over $TiO_2$, Saladin et al. showed that the rate of methane formation increases upon going from 20 to 200 °C, indicating the rate-determining step is a thermal process (41, 42). Significantly, no higher $C_n$ products were reported, which we suspect is because they lacked a proper FTS cocatalyst, such as cobalt. In our current system, the kinetics of the carbon-chain-forming reactions seem to be rate-determining at ~200 °C. Higher temperatures may yield further improvement but it should be noted that the selectivity of cobalt-based FTS catalysts for higher $C_n$ products peaks in the 200–220 °C region (43).

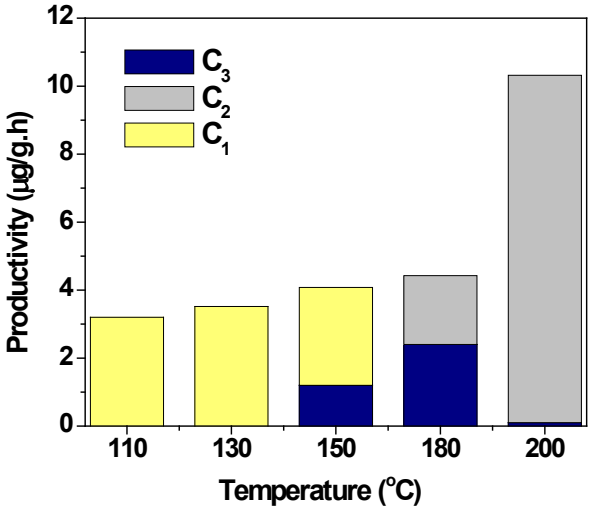


**Fig. 2.** Mass productivity and $C_n$ selectivity as a function of photothermal reactor temperature at 1 bar and $P_{H2O}/P_{CO2}$ =1.2, and 40 sccm.

**Table 1. Products and mass and molar electron productivity as a function of pressure and partial pressure ratio at a constant temperature of 200 °C and flow rate of 40 sccm**

| | Mass productivity, $P_m$, μg/gh | | | | | | Molar productivity, $P_{mol}$, μmole/gh | | | | | |
|---|---|---|---|---|---|---|---|---|---|---|---|---|
| $P(H_2O)/P(CO_2)$ | 0.6 | | | 1.2 | | | 0.6 | | | 1.2 | | |
| Pressure | 1.0 | 2.7 | 6.1 | 1.0 | 2.7 | 6.1 | 1.0 | 2.7 | 6.1 | 1.0 | 2.7 | 6.1 |
| Compound | $P_m$ | $P_m$ | $P_m$ | $P_m$ | $P_m$ | $P_m$ | $P_{mol}$ | $P_{mol}$ | $P_{mol}$ | $P_{mol}$ | $P_{mol}$ | $P_{mol}$ |
| $O_2$ | 195 ± 149 | 308 ± 118 | 171 ± 140 | 194 | 138 | 307 | 24 ± 19 | 39 ± 15 | 21 ± 18 | 24 | 33 | 38 |
| $H_2$ | 8 ± 9 | 14 ± 4 | 6 ± 2 | 6 | 20 | 10 | 8 ± 9 | 14 ± 4 | 6 ± 2 | 6 | 18 | 10 |
| $C_1$ | 23 ± 12 | 44 ± 63 | 55 ± 72 | 8 | 4 | 28 | 2 ± 1 | 4 ± 4 | 4 ± 5 | 1 | 3 | 2 |
| $C_{2-4}$ | 26 ± 17 | 76 ± 40 | 91 ± 79 | 28 | 6 | 60 | 7 ± 5 | 15 ± 11 | 19 ± 17 | 10 | 13 | 13 |
| $C_5$+ | 4 ± 5 | 7 ± 11 | 22 ± 13 | 0 | 0 | 0 | 1 ± 2 | 4 ± 5 | 5 ± 8 | 0 | 1 | 0 |
| Total | 61 ± 5 | 141 ± 27 | 175 ± 39 | 43 | 30 | 98 | 18 ± 3 | 36 ± 3 | 35 ± 6 | 17 | 35 | 26 |
| $O_2$ yield | | | | | | | 136 | 108 | 62 | 140 | 94 | 150 |
| Select prod | | | | | | | | | | | | |
| $C_5H_{12}O$ | 3.7 ± 5.2 | 1.6 ± 1.9 | 1.7 ± 2.1 | 0.0 | 0.0 | 0.0 | 1.3 ± 1.8 | 0.8 ± 0.7 | 0.6 ± 0.7 | 0.0 | 0.0 | 0.0 |
| $C_7H_{12}$ | 0 | 0.4 ± 0.6 | 0.0 | 0.0 | 0.0 | 0.0 | 0.0 | 0.2 ± 0.3 | 0.0 | 0.0 | 0.0 | 0.0 |
| $C_8H_{18}$ | 0 | 0.4 ± 0.6 | 0.0 | 0.0 | 0.0 | 0.0 | 0.0 | 0.2 ± 0.3 | 0.0 | 0.0 | 0.0 | 0.0 |
| $C_8H_{16}O_5$ | 0 | 0.0 | 2.2 ± 3.8 | 0.0 | 0.0 | 0.0 | 0.0 | 0.0 | 0.4 ± 0.8 | 0.0 | 0.0 | 0.0 |
| $C_9H_{12}$ | 0 | 0.6 ± 1.1 | 0.0 | 0.0 | 0.0 | 0.0 | 0.0 | 0.0 | 0.0 | 0.0 | 0.0 | 0.0 |
| $C_{10}H_{20}O_2$ | 0 | 0.4 ± 0.8 | 0.5 ± 1.1 | 0.0 | 0.0 | 0.0 | 0.0 | 0.3 ± 0.4 | 0.7 ± 0.2 | 0.0 | 0.0 | 0.0 |
| $C_{13}H_{12}$ | 0 | 0.9 ± 1.5 | 0.0 | 0.0 | 0.0 | 0.0 | 0.0 | 0.5 ± 0.7 | 0.0 | 0.0 | 0.0 | 0.0 |

Temperatures higher than this quickly lead to losses in the desired selectivity and corresponding increases in methanation.

Further experiments were run at 200 °C at three total pressures (1.0, 2.7, and 6.1 bar) and two partial pressure ratios: $P_{H2O}/P_{CO2}$ = 0.6 and 1.2. These data are collected in Table 1, which reports the mean productivity for each run, in units of mass productivity ($\mu g_{prod} \cdot g^{-1}_{cat} \cdot h^{-1}$) and molar productivity ($\mu mol_e \cdot g^{-1}_{cat} \cdot h^{-1}$, where $\mu mol_e$ = μmol electrons stored in the product). The products are divided into $O_2$, $H_2$, $C_1$, $C_2$–$C_4$, and $C_5$+, with certain higher $C_n$ products explicitly listed. For data in which SDs are reported, the values are the mean of three independents runs, whereas those without are single-run data. The full product distribution and productivity data are given in *SI Appendix*, Tables S4 and S5. Fig. 3 is a bar graph comparing the mass productivity and selectivity as a function of pressure and feedstock ratio. The most compelling data are the observation that the $C_2$+ hydrocarbons and oxygenates are not minor products but instead constitute 74% by mass of the products under one of the best set of conditions screened (6.1 bar, $P_{H2O}/P_{CO2}$ = 0.6). Converted to a molar basis (moles of reducing electrons stored in products), this amounts to 68% of all electrons stored in products in $C_2$+ hydrocarbons. Of this, 22% by mass and 14% of the electrons are stored in liquid $C_5$+ products. The $H_2$ and $C_1$ products account for 35% of product mass and 29% of all electrons stored, but they are not the dominant products. In both feedstock ratios, we clearly observe an increase in overall productivity with increasing total pressure. However, only at the lower $P_{H2O}/P_{CO2}$ of 0.6 do we observe any $C_5$+ selectivity which becomes more favorable with increasing pressure. Clearly, the feedstock ratio is an important parameter that merits further investigation and optimization. These data reveal, to a first approximation, that the SPARC reaction responds to temperature and pressure in a manner similar to the FTS reaction and yields similar products. It is well-known that the FTS reaction responds to increases in pressure with an increase in productivity (gram product per gram catalyst per hour) and a shift in product distribution (selectivity) toward heavier hydrocarbons (40), and that the optimized industrial conditions are generally given around 20 atm, 220 °C, with a 2:1 ratio of $H_2$ and CO for a cobalt-based catalyst (44, 45). Because of this, we believe it is reasonable to assume some shared underlying chemical mechanisms and assume that higher pressures will shift the selectivity in SPARC chemistry to favor higher $C_n$ products. Our current reactor could not safely go beyond 6.1 bar; however, we are fabricating a next-generation photoreactor able to withstand both higher pressures and temperatures.

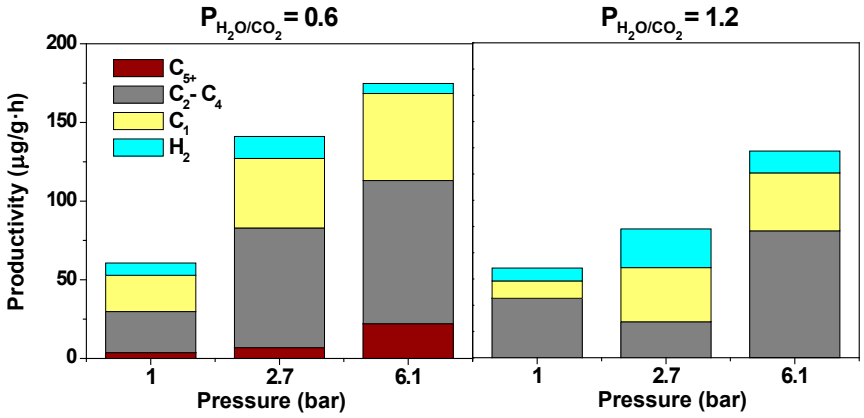


**Fig. 3.** Mass productivity and selectivity of SPARC reaction at different pressure and partial pressure ratios at 200 °C and 40 sccm.

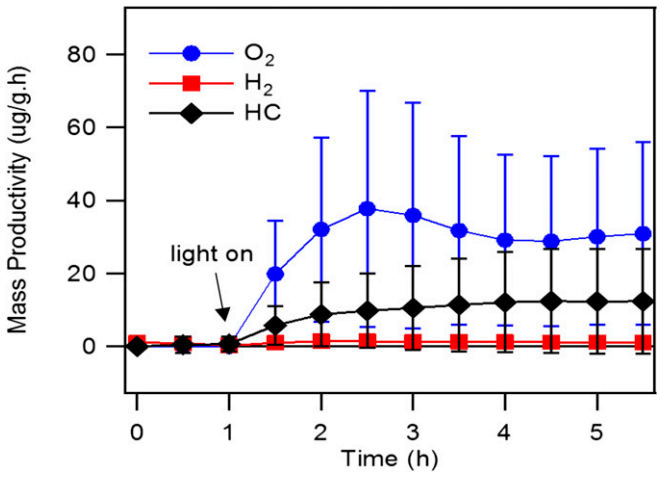


**Fig. 4.** Productivity of $O_2$ (blue circles) $H_2$ (red squares), and hydrocarbons (HC) (black diamonds) as a function of time at 200 °C, 6.1 bar, $P_{H2O}/P_{CO2} = 0.6$ and 40 sccm.

The percentage of oxygenates in our product distribution at 70–90% by mass is much higher than found in typical FTS chemistry. This is, perhaps, not too surprising in that SPARC reactants are considerably richer in oxygen content. As water is a reactant in SPARC chemistry, $P_{H2O}$ is expected to have a strong influence on the observed chemistry compared with the secondary effects which arise from water in FTS chemistry. At high $P_{H2O}$ the SPARC reaction can presumably produce a great deal of $H_2$ or hydride equivalents, which should be advantageous, but water is also better able to bind to the surface than $CO_2$ due to its polar nature and strong H-bonding properties; therefore, high $P_{H2O}$ can saturate the surface, blocking effective $CO_2$ adsorption and reducing hydrocarbon production. Just recently, Rani et al. showed that (Cu, Pt)–$TiO_2$-based photoreduction of $CO_2$ to $CH_4$ and CO at ambient temperature was maximized at 50% humidity and dropped at higher levels, presumably due to water-blocking surface binding of the $CO_2$ (46). FTS is technically run with zero $P_{H2O}$ but because water is a product, some is always present. At low $P_{H2O}$, the SPARC reaction may be starved for hydride equivalents, leading to incomplete reduction of the $CO_2$. Surprisingly, a number of FTS studies have shown that deliberate addition of water to the feed can be beneficial in terms of shifting the selectivity toward $C_5$+ products (14–17), which indicates that the presence of water, in itself, is not detrimental to the hydrocarbon-chain-forming process. It is not yet clear how the selectivity of the SPARC reaction can be tuned toward less-oxygenated products, but the feedstock ratio is likely to be one key factor. In any case, most of these oxygenates are high molecular weight molecules with a greater fuel value on a mass basis than lighter alcohols or oxygenates.

Isotopic labeling experiments performed with $^{13}CO_2$ and $D_2O$ feedstocks show incorporation of both labels into all of the reduced products (*SI Appendix*). The $O_2$ yields, shown in Table 1, were calculated by dividing all of the electrons released to form $O_2$ from $H_2O$ by all of the electrons stored in the identified products at the expected stoichiometry for the SPARC reaction and range from 64% to 150%. The agreement is acceptable considering the large SDs in these measurements, which reflect difficulties in obtaining good peak integration due to large adjacent $CO_2$ and $N_2$ peaks in the chromatogram (*SI Appendix*, Fig. S6).

As seen in Fig. 4, no $O_2$ and only trace hydrocarbons are detected before the catalyst bed is irradiated. Although difficult to see, there is a small amount of $H_2$, $CH_4$, and $C_2H_6$, produced during the dark period, constituting less than 10% of the $CH_4$ and $C_2H_6$ observed once the light is on. These basal products are attributed to thermal reactions of $H_2O$ and $CO_2$ with the freshly prepared and highly reactive nanosized cobalt islands (catalyst preparation and characterization are given in the *SI Appendix*), some of which are unstable toward oxidation. When the catalyst is irradiated there is a substantial increase in HC, $H_2$, and $O_2$ productivity consistent with a coupling of photochemical water oxidation with thermal $CO_2$ and proton reduction. Furthermore, the productivity is reasonably stable over the run period; however, transmission electron microscopy (TEM) analyses of the catalyst pre- and postrun reveal substantial agglomeration of the cobalt islands over this period (*SI Appendix*, Fig. S2). The initial cobalt islands averaging 4.5 ± 2.0 nm in diameter approximately doubled in size to 9.7 ± 2.5 nm over the 5-h run timeframe. Cobalt-based FTS catalysts undergo considerable reorganization in the first 24 h of on-stream use (47, 48) and it seems that a similar reorganization is occurring here. However, given the early stage of SPARC chemistry and our current limit on short time runs (5–8 h), there are not yet enough data to fully understand the catalyst behavior here. This will certainly be explored as we examine the catalyst stability and evolution over longer time periods.

Table 1 also lists the productivity data for select $C_5$+ products, whose structures are shown in Fig. 5. The structures were determined by National Institute of Standards & Technology (NIST) database matching of the mass spectrum fragmentation patterns and were fit with confidence level greater than 99% for nearly all compounds. $C_5H_{12}O$ and $C_8H_{18}$ are two saturated hydrocarbons typical of an FTS-like mechanism. The alkylbenzenes or oxygenates thereof suggest formation of surface acetylides/acetylenes, which can easily undergo cyclotrimerization to lead to the observed products (49). This second C–C chain-forming pathway is reasonable if we consider that the SPARC reaction conditions are considerably less hydrogen-rich relative to normal FTS, which rarely yields alkynes. Whereas this unexpected mechanism seems to be responsible for the aromatic $C_6$+ products, the presence of $C_8H_{18}$ as well as $C_7$ and $C_5$ alkanes and olefins supports an FTS process is occurring concurrently.

The highest mass productivity obtained, 200 °C, 6.1 bar, $P_{H2O}/P_{CO2} = 0.6$, corresponded to 175 $\mu g \cdot g^{-1} \cdot h^{-1}$, not including $O_2$, or a molar electron productivity of 35 $\mu mol_e \cdot g^{-1} \cdot h^{-1}$. For comparisons, this latter value is ~20 $\mu mol\ H_{2(equiv)} g^{-1} \cdot h^{-1}$ and is within the typical range of the 0.2–100-$\mu mol\ product \cdot g^{-1} \cdot h^{-1}$ (50, 51), reported for $CO_2/H_2O$ semiconductor photocatalysis, although claims as high as 2,000 $\mu mol\ ethanol\ g^{-1} \cdot h^{-1}$ exist (52). When examined with respect to the incident photon flux ($\lambda \leq 400$ nm), an incident photon quantum yield (IPQY) of 0.02–0.05% is obtained on a per electron stored basis. These IPQYs are slightly higher if reported relative to the $O_2$ yield. Unfortunately, many studies of $CO_2/H_2O$ semiconductor photocatalysis either do not report quantum yields or do not report them in a consistent manner. Where data exist, typical IPQY values are anywhere from 0.001% to 30%, although the higher values (>1%) were only seen with

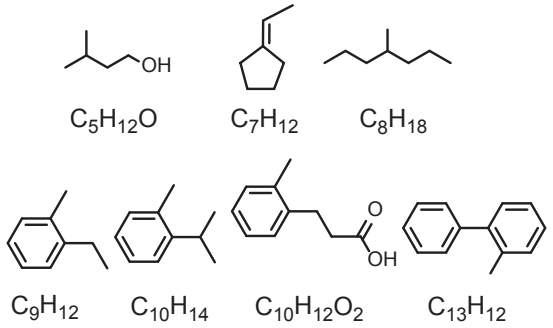


**Fig. 5.** Structures of select $C_5$+ products as determined from NIST mass spectral database.

nonoxide catalysts (i.e., ZnS, CdS, GaP) (24). We suggest that our modest IPQY is more a reflection of the early stage of this work rather than any practical limitation and note that a significant (2.5-fold) jump in IPQY was observed upon increasing the pressure from 1 to 2.7 bar; however, no further increase was seen at 6.1 atm.

As mentioned previously, the choice of a good metal for FTS catalyst is crucial and Fe, Co, and Ru are among the best known (39). Here, we chose cobalt due to its known FTS performance and superior stability relative to iron (44), and to demonstrate that the SPARC reaction could be achieved without the requirement of rare or precious metal cocatalysts. In one of the few studies of the $CO_2/H_2O$ semiconductor photocatalysis at temperatures in excess of 100 °C, only $C_1$ products were found with copper and platinum zincates and titanate photocatalysts (53). However, when Fe was used in the same systems, ethanol in addition to the $C_1$ products was observed (54), suggesting the SPARC reaction was in operation. It is curious that even higher $C_n$ products were not observed, but these photoreactions were conducted at temperatures in excess of 300 °C, which may well be too high for good operation. Oddly enough, cobalt-based catalysts yield primarily methane during the hydrogenation of $CO_2$ (55, 56). It was also shown that the increased water partial pressure stabilized the catalyst and it may be that the even higher $P_{H2O}$ is influencing the SPARC product distribution here.

In general, elevated temperatures are avoided in photochemical reactions due to increased rates of charge recombination in the photocatalyst. For example, the photoluminescence intensity of $TiO_2$ drops by 50–60% upon raising the temperature from 20 to 200 °C (57, 58). At present, we observe an increase in productivity with temperature, showing a significant thermal component to the rate-determining kinetic step in this photothermochemical reaction. Nonetheless, the losses in charge carriers could be an important consideration upon development of an improved SPARC catalyst, where the thermal steps are no longer rate-determining.

At present, this gas-phase SPARC reaction is far from optimized and simply shows proof of principle. Higher productivities and better product distributions are likely to be realized as pressure, temperature, reactant ratio, space velocity, and catalyst are optimized. For example, the current photoreactor can only safely be operated at pressures less than 6.1 bar, whereas higher pressures are likely to dramatically affect product selectivity and productivity. Similarly, Brunauer–Emmett–Teller (BET) surface area measurements reveal that the Nafion polymer, used to bind the catalyst powder to the glass beads, effectively covers up 50–60% of the catalyst surface area (*SI Appendix*), revealing that we can likely do better using alternative methods to immobilize the catalyst. The current data also raise a number of important questions which must be addressed if this technology is to be further developed. As both $H_2$ and CO are observed in the product stream, it is not clear if they are responsible for hydrocarbon formation via the FTS upon readsorption or if they represent a small fraction of surface escaped species. The most commonly invoked mechanism for metal cocatalysts on photoactive $TiO_2$ is that the metal islands act as electron collectors upon which metal hydrides and $CO_2$ adsorption/reduction occurs, whereas the holes migrate to the $TiO_2$ surface where they oxidize water. In a gas-phase model, the protons must migrate over the surface of the $TiO_2$ to the cobalt islands, leading to questions about the degree of surface hydration. It is notable that in the hydrogenation of CO or $CO_2$ on cobalt metal, several common surface-bound intermediates are invoked, even though the former gives hydrocarbon chains and the latter gives methane (55, 56).

Although the current SPARC technology is currently impractical on a commercial scale, it does offer a conceptually new and commercially promising solar fuels technology that would be simple and inexpensive relative to most PV-EC and PEC systems. The direct production of the value-added hydrocarbons liquid fuel minimizes the number of unit operations involved and the associated efficiency losses and capital expenses of each. In a field operation, it is easy to imagine the use of parabolic mirrors to focus and concentrate sunlight onto a catalyst bed, providing both the photons required for photoexcitation and the thermal energy needed to run the reaction. Assuming such a system may require active cooling, the excess thermal energy could be used for downstream product separations or other applications in which relatively low-grade heat can be applied. In this respect, an SPARC process can realize greater efficiencies than process requiring ambient or near-ambient temperatures in that the low-energy photons are used to help heat the SPARC reaction and to heat a working fluid to a more useful temperature (i.e., 200 °C). Concentrated sunlight minimizes photocatalyst costs and reactor volume, the former of which is often one of the more expensive components of any such technology. Another significant economic consideration of the process SPARC is that it is not expensive to compress $CO_2$ and $H_2O$ and a liquid product is produced. Solar biomass gasification and related processes which produce CO and $H_2$ will subsequently require expensive compression to convert these gases to usable solar fuels. Finally, the SPARC reaction, as realized here, is a true gas-phase operation operating at conditions more typical of an industrial operation. The elevated temperature, pressure, and gas-phase operation also open previously unidentified possibilities about the types of semiconductors catalysts that are needed and may be used.

## Materials and Methods

The 5% cobalt on Degussa P25 $TiO_2$ was prepared by wet impregnation of the $TiO_2$ with $Co(NO_3)_2$, calcining at 250 °C for 3 h. This precatalyst was mixed in water/propanol with Nafion D521 polymer and coated onto surface-roughened 2-mm Pyrex glass beads, which were then isolated and dried for 4 h at 100 °C. The dried coated beads were loaded into the flow reactor shown in Fig. 1 and the catalyst activated by reduction with flowing $H_2$ at 350 °C for 12 h. The catalyst was characterized right after reduction and postrun by BET surface area measurements, TEM, and X-ray photoelectron spectroscopy. Products captured in the condenser were analyzed at the end of the reaction by extraction into dichloromethane and analyzed by GC-MS. Gaseous products were analyzed every 30 min using an online GC. Full experimental details for the reactor design and function, catalyst preparation and characterization, product identification, yield and distribution, and isotopic labeling are given in the *SI Appendix*.

**ACKNOWLEDGMENTS.** We thank Dr. Upendra Joshi helpful discussions and help with reviewing the manuscript. We also thank the reviewers for many helpful comments that greatly improved this manuscript. The National Science Foundation (CHE-1301332), Robert A. Welch Foundation (Y-1301), and the University of Texas at Arlington Center for Renewable Science and Technology (CREST) are gratefully acknowledged for financial support.

1. Armaroli N, Balzani V (2010) Solar fuels. *Energy for a Sustainable World* (Wiley-VCH, Weinheim, Germany), pp 203–229.
2. Solomon SD, et al., eds (2007) *Climate Change 2007 - The Physical Science Basis*. Working Group I Contribution to the Fourth Assessment Report of the IPCC (Cambridge Univ Press, Cambridge, UK), p 1009.
3. Solomon S, Plattner G-K, Knutti R, Friedlingstein P (2009) Irreversible climate change due to carbon dioxide emissions. *Proc Natl Acad Sci USA* 106(6):1704–1709.
4. Lewis NS, Nocera DG (2006) Powering the planet: Chemical challenges in solar energy utilization. *Proc Natl Acad Sci USA* 103(43):15729–15735.
5. Torella JP, et al. (2015) Efficient solar-to-fuels production from a hybrid microbial-water-splitting catalyst system. *Proc Natl Acad Sci USA* 112(8):2337–2342.
6. Song W, et al. (2011) Making solar fuels by artificial photosynthesis. *Pure Appl Chem* 83(4):749–768.
7. Liu C, et al. (2015) Nanowire-bacteria hybrids for unassisted solar carbon dioxide fixation to value-added chemicals. *Nano Lett* 15(5):3634–3639.
8. Steinfeld A (2005) Solar thermochemical production of hydrogen—a review. *Sol Energy* 78(5):603–615.
9. Cox CR, Lee JZ, Nocera DG, Buonassisi T (2014) Ten-percent solar-to-fuel conversion with nonprecious materials. *Proc Natl Acad Sci USA* 111(39):14057–14061.
10. Barbir F (2005) PEM electrolysis for production of hydrogen from renewable energy sources. *Sol Energy* 78(5):661–669.

11. Kamat PV, Tvrdy K, Baker DR, Radich JG (2010) Beyond photovoltaics: Semiconductor nanoarchitectures for liquid-junction solar cells. *Chem Rev* 110(11):6664–6688.
12. Kumar B, et al. (2012) Photochemical and photoelectrochemical reduction of $CO_2$. *Annu Rev Phys Chem* 63(1):541–569.
13. Walter MG, et al. (2010) Solar water splitting cells. *Chem Rev* 110(11):6446–6473.
14. Hisatomi T, Kubota J, Domen K (2014) Recent advances in semiconductors for photocatalytic and photoelectrochemical water splitting. *Chem Soc Rev* 43(22): 7520–7535.
15. Grätzel M, ed (1983) *Energy Resources Through Photochemistry and Catalysis* (Academic, New York).
16. Alibabaei L, et al. (2013) Applications of metal oxide materials in dye sensitized photoelectrosynthesis cells for making solar fuels: Let the molecules do the work. *J Mater Chem A* 1(13):4133–4145.
17. Alibabaei L, Sherman BD, Norris MR, Brennaman MK, Meyer TJ (2015) Visible photoelectrochemical water splitting into $H_2$ and $O_2$ in a dye-sensitized photoelectrosynthesis cell. *Proc Natl Acad Sci USA* 112(19):5899–5902.
18. The Hydrogen Economy (2004) *Opportunities, Costs, Barriers, and R&D Needs* (The National Academies Press, Washington, DC), p 256.
19. Centi G, Quadrelli EA, Perathoner S (2013) Catalysis for $CO_2$ conversion: A key technology for rapid introduction of renewable energy in the value chain of chemical industries. *Energy Environ Sci* 6:1711–1731.
20. van der Giesen C, Kleijn R, Kramer GJ (2014) Energy and climate impacts of producing synthetic hydrocarbon fuels from CO(2). *Environ Sci Technol* 48(12):7111–7121.
21. Halmann M (1978) Photoelectrochemical reduction of aqueous carbon dioxide on p-type GaP in liquid junction solar cells. *Nature* 275(5676):115–116.
22. Inoue T, Fujishima A, Konishi S, Honda K (1979) Photoelectrocatalytic reduction of carbon dioxide in aqueous suspensions of semiconductor powders. *Nature* 277(5698): 637–638.
23. Chen X, Shen S, Guo L, Mao SS (2010) Semiconductor-based photocatalytic hydrogen generation. *Chem Rev* 110(11):6503–6570.
24. Habisreutinger SN, Schmidt-Mende L, Stolarczyk JK (2013) Photocatalytic reduction of $CO_2$ on $TiO_2$ and other semiconductors. *Angew Chem Int Ed Engl* 52(29):7372–7408.
25. Hwang J-S, Chang J-S, Park S-E, Ikeue K, Anpo M (2005) Photoreduction of carbon dioxide on surface functionalized nanoporous catalysts. *Top Catal* 35(3-4):311–319.
26. Kubacka A, Fernández-García M, Colón G (2012) Advanced nanoarchitectures for solar photocatalytic applications. *Chem Rev* 112(3):1555–1614.
27. Ashford DL, et al. (2015) Molecular chromophore–catalyst assemblies for solar fuel applications. *Chem Rev* 115(23):13006–13049.
28. Song W, et al. (2013) Visualization of cation diffusion at the $TiO_2$ interface in dye sensitized photoelectrosynthesis cells (DSPEC). *Energy Environ Sci* 6(4):1240–1248.
29. Hoffmann MR, Moss JA, Baum MM (2011) Artificial photosynthesis: Semiconductor photocatalytic fixation of $CO_2$ to afford higher organic compounds. *Dalton Trans* 40(19):5151–5158.
30. Mizuno T, Adachi K, Ohta K, Saji A (1996) Effect of $CO_2$ pressure on photocatalytic reduction of $CO_2$ using $TiO_2$ in aqueous solutions. *J Photochem Photobiol Chem* 98: 87–90.
31. Xia X-H, et al. (2007) Preparation of multi-walled carbon nanotube supported $TiO_2$ and its photocatalytic activity in the reduction of $CO_2$ with $H_2O$. *Carbon* 45(4): 717–721.
32. Subrahmanyam M, Kaneco S, Alonso-Vante N (1999) A screening for the photo reduction of carbon dioxide supported on metal oxide catalysts for $C_1$-$C_3$ selectivity. *Appl Catal B* 23:169–174.
33. Barton EE, Rampulla DM, Bocarsly AB (2008) Selective solar-driven reduction of $CO_2$ to methanol using a catalyzed p-GaP based photoelectrochemical cell. *J Am Chem Soc* 130(20):6342–6344.
34. Cole EB, et al. (2010) Using a one-electron shuttle for the multielectron reduction of $CO_2$ to methanol: Kinetic, mechanistic, and structural insights. *J Am Chem Soc* 132(33): 11539–11551.
35. Roy SC, Varghese OK, Paulose M, Grimes CA (2010) Toward solar fuels: Photocatalytic conversion of carbon dioxide to hydrocarbons. *ACS Nano* 4(3):1259–1278.
36. Varghese OK, Paulose M, Latempa TJ, Grimes CA (2009) High-rate solar photocatalytic conversion of $CO_2$ and water vapor to hydrocarbon fuels. *Nano Lett* 9(2):731–737.
37. Pendyala V, Shafer W, Davis B (2013) Aqueous-phase Fischer–Tropsch synthesis: Effect of reaction temperature on ruthenium nanoparticle catalyst and comparison with supported Ru and Co catalysts. *Catal Lett* 143(9):895–901.
38. Zennaro R, Tagliabue M, Bartholomew CH (2000) Kinetics of Fischer–Tropsch synthesis on titania-supported cobalt. *Catal Today* 58(4):309–319.
39. Vannice MA (1975) The catalytic synthesis of hydrocarbons from $H_2CO$ mixtures over the group VIII metals: I. The specific activities and product distributions of supported metals. *J Catal* 37(3):449–461.
40. James OO, Chowdhury B, Mesubi MA, Maity S (2012) Reflections on the chemistry of the Fischer-Tropsch synthesis. *RSC Adv* 2(19):7347–7366.
41. Saladin F, Alxneit I (1997) Temperature dependence of the photochemical reduction of $CO_2$ in the presence of $H_2O$ at the solid gas interface of $TiO_2$. *Journal of the Chemical Society, Faraday Transactions* 93(23):4159–4163.
42. Saladin F, Forss L, Kamber I (1995) Photosynthesis of $CH_4$ at a $TiO_2$ surface from gaseous $H_2O$ and $CO_2$. *J Chem Soc Chem Commun* 5:533–534.
43. Dry ME (1981) *Catalysis Science and Technology*, eds Anderson JR, Boudart M (Springer, New York), Vol 1, p 159.
44. Khodakov AY, Chu W, Fongarland P (2007) Advances in the development of novel cobalt Fischer-Tropsch catalysts for synthesis of long-chain hydrocarbons and clean fuels. *Chem Rev* 107(5):1692–1744.
45. Visconti CG, Mascellaro M (2013) Calculating the product yields and the vapor–liquid equilibrium in the low-temperature Fischer–Tropsch synthesis. *Catal Today* 214:61–73.
46. Rani S, Bao N, Roy SC (2014) Solar spectrum photocatalytic conversion of $CO_2$ and water vapor into hydrocarbons using $TiO_2$ nanoparticle membranes. *Appl Surf Sci* 289:203–208.
47. Karaca H, et al. (2010) In situ XRD investigation of the evolution of alumina-supported cobalt catalysts under realistic conditions of Fischer-Tropsch synthesis. *Chem Commun (Camb)* 46(5):788–790.
48. Khodakov AY (2009) Fischer-Tropsch synthesis: Relations between structure of cobalt catalysts and their catalytic performance. *Catal Today* 144(3–4):251–257.
49. Vollhardt KPC (1984) Cobalt-mediated [2+ 2+ 2]-cycloadditions: A maturing synthetic strategy. *Angew Chem Int Ed Engl* 23(8):539–556.
50. Izumi Y (2013) Recent advances in the photocatalytic conversion of carbon dioxide to fuels with water and/or hydrogen using solar energy and beyond. *Coord Chem Rev* 257(1):171–186.
51. Mao J, Li K, Peng T (2013) Recent advances in the photocatalytic $CO_2$ reduction over semiconductors. *Catal Sci Technol* 3(10):2481–2498.
52. Liu Y, et al. (2009) Selective ethanol formation from photocatalytic reduction of carbon dioxide in water with $BiVO_4$ photocatalyst. *Catal Commun* 11(3):210–213.
53. Guan G, Kida T, Harada T, Isayama M, Yoshida A (2003) Photoreduction of carbon dioxide with water over $K_2Ti_6O_{13}$ photocatalyst combined with Cu/ZnO catalyst under concentrated sunlight. *Appl Catal A* 249(1):11–18.
54. Guan G, Kida T, Yoshida A (2003) Reduction of carbon dioxide with water under concentrated sunlight using photocatalyst combined with Fe-based catalyst. *Appl Catal B* 41(4):387–396.
55. Visconti CG, et al. (2009) Fischer–Tropsch synthesis on a $Co/Al_2O_3$ catalyst with $CO_2$ containing syngas. *Appl Catal A* 355(1):61–68.
56. Zhang Y, Jacobs G, Sparks DE, Dry ME, Davis BH (2002) CO and $CO_2$ hydrogenation study on supported cobalt Fischer–Tropsch synthesis catalysts. *Catal Today* 71(3): 411–418.
57. Forss L, Schubnell M (1993) Temperature dependence of the luminescence of $TiO_2$ powder. *Appl Phys B* 56:363–366.
58. Schubnell M, Kamber I, Beaud P (1997) Photochemistry at high temperatures - potential of ZnO as a high temperature photocatalyst. *Appl Phys, A Mater Sci Process* 64: 109–113.